A Multilayer Perception Trained Method in Speed Control of a Linear Switched Reluctance Motor

Siamak Masoudi, *Member, IEEE*, and Hasan Mehrjerdi, *Senior Member, IEEE*

***Abstract*—Switched reluctance motors are nonlinear systems with some uncertainties and unmodeled dynamics. Propulsion force and speed in these motors have inherently high fluctuations complicating their applications. The conventional controllers could not offer a precise performance for nonlinear systems because they require analytical calculations of the partial derivatives. Accordingly, in this article, a multilayer perception is presented to overcome this problem and control a linear motor. Training algorithms require a complete dataset of the system output, which complicates their implementation. To solve this problem, a Kalman filter is used to estimate uncertain parameters. Thus, the proposed control system does not require a complete dataset of the system. It can process data and predict the next values in a short time without complete observations. The proposed control strategy is implemented to a linear switched reluctance motor and the results are compared with two other conventional methods via simulation and experimental tests. The results confirm the ability and accuracy of the proposed method.**

***Index Terms*—.**

I. Introduction

SWITCHED reluctance motors (SRMs) are attractive electrical machines with many advantages such as single excitation, simple construction, low cost, and wide speed range performance. In applications, such as electric trains and elevators where motion is in a direct path, linear-type motors can be very useful by eliminating mechanical converters. This is very effective in simplicity of construction and cost of the system. Due to the special construction, propulsion force or torque in SRMs inherently has a noticeable ripple, which limits their applications. SRMs are completely nonlinear systems making it more difficult to model their dynamic behavior. In addition, they suffer from some uncertainties that should be updated in the performance process. The results of finite element analysis (FEA) can be helpful in the motor dynamic behavior [1]. In some studies, the inductance profile of an SRM has been indicated by an equation. A practical method to determine the real-time characteristics of SRMs has been presented in [2], which is efficient in the real-time emulation and the performance evaluation of the motors.

The conventional proportional–integral derivative (PID) controller offers many features, such as fast control, shorter settling time, and low-cost application, but it has less stability. To overcome this, a fractional-order PI speed controller for an SRM has been proposed in [3]. Another modified PI control strategy with self-tuning has been presented in [4]. When using a PI controller, the parameters and other uncertainties, such as external disturbances and the input constraints, affect the transient performance of the drive system. To overcome this, an improved PI speed controller capable of preserving almost the nominal transient performance has been indicated in [5]. To overcome the parameter uncertainty and external disturbances, a reduced-order PI controller has been addressed in [6]. Different studies have presented algorithms to obtain gains of a PI controller. Classical PI speed controller has been employed in a double-sided LSRM in [7].

A new control strategy has been presented in [8], which is based on the developed flux modulation principle. In sensorless SRM drives, parameter uncertainty, voltage drop on power devices, and resistance changes affect the accuracy of the control system. A new inductance calculation method has been proposed in [9] to overcome the uncertainty of the parameter. A nonlinear state observer for control of SRM drives over medium- and high-speed ranges has been proposed in [10], which has acceptable robustness against flux linkage distortions. In an SRM with some parameter uncertainties and changes in operation conditions, controller constants must be tuned instantly to achieve a high level of performance. An adaptive control system is one in which the controller parameters are adjusted automatically to compensate for altering process conditions. We have presented an adaptive control method in combination with a fuzzy system in [11] and with a sliding mode method in [12] for an LSRM. In [13], a classical PI control has been improved using an adaptive method and a self-tuning strategy. To control a nonlinear system with some uncertainties, a simple adaptive PI control method has been proposed in [14]. The controller has been utilized as a speed controller for an electric vehicle to track the desired command speed. Adaptive control strategy has been applied to overcome the uncertainty of parameters in position control of an SRM in [15]. To update the control parameters of a linear SRM, an adaptive method along with a genetic algorithm have been used in [16]. A comprehensive analysis of torque ripple and power factor for three-phase SRM fed by sinusoidal current excitation has been presented in [17] and [18].

Manuscript received May 9, 2021; revised June 20, 2021 and September 7, 2021; accepted November 1, 2021. Date of publication November 8, 2021; date of current version December 31, 2021. Recommended for publication by Associate Editor U. Deshpande. *(Corresponding author: Siamak Masoudi.)*

Siamak Masoudi is with the Department of Electrical Engineering, Abhar Branch, Islamic Azad University, Abhar, Iran (e-mail: s.masoudi@tabrizu.ac.ir).

Hasan Mehrjerdi is with the Department of Electrical Engineering, Qatar University, Doha, Qatar (e-mail: hasan.mehrjerdi@qu.edu.qa).

Color versions of one or more figures in this article are available at https://doi.org/10.1109/TPEL.2021.3125606.

Digital Object Identifier 10.1109/TPEL.2021.3125606

The Kalman filter (KF) is a data fusion algorithm that predicts the next state vector of parameters based on previous information of the system and the current measurements. An overview of a KF applied to control ac motors has been provided in [19]. In [20], a KF has been used with a neural controller to obtain an accurate induction motor model, which is robust to external disturbances and parameter variations. An adaptive KF with offline parameter and observer design optimization has been proposed in [21] to obtain the accurate motor model including magnetic saturation, iron losses, and skin effect influences.

The use of KF in SRM control has been shown in [22]. The method needs no sensors to determine the speed and position of the rotor. Another research dealt with sensorless position control of an 8/6 SRM with uncertainties in load torque [23] that an extended KF has been applied along with a second-order sliding mode observer. A general sensorless control strategy for a linear SRM has been introduced in [24]. The method describes how to find out the position of the translator using two cascading discrete KFs to estimate the speed and position.

In this article, an adaptive PI controller along with an extended KF has been used to control the speed of an LSRM. The proposed control system can adapt to uncertainties of parameters while not requiring complete information about the system outputs. In Section II, the proposed LSRM and its dynamic curves have been introduced and a general control system has been demonstrated, which includes a speed regulator. Details of the multilayer perception (MLP) trained method and the extended KF have been discussed in Section III. The simulation and experimental results have been shown in Section IV. Finally, Section V concludes this article.

II. Prototype LSRM

A. Motor Structure

A four-phase double-sided linear SRM (LSRM) has been studied in this article. In the motor, two phases are fed simultaneously resulting in a high density of the propulsion force with significantly fewer ripples. These features have made the motor acceptable for many applications, such as electric trains. The proposed LSRM and its characteristics are shown in Fig. 1.

B. Dynamic Equations

For any phase of the LSRM, the voltage equation is written as

$$v_k = Ri_k + \frac{d\lambda_k}{dt}, \quad \lambda_k = L_k\ (i_k, x)\ .i_k \tag{1}$$

$$\frac{d\lambda_k}{dt} = L_k\ (i_k, x)\ \frac{di_k}{dt} + g_k.v_x.i_k \tag{2}$$

where v_k, i_k, and λ_k denote the voltage, current, and linkage flux, respectively, whereas R and $\mathrm{L_k}$ indicate the winding resistance and inductance of any phase, respectively. In addition, $v_x = dx/dt$ is linear speed and $g_k = dL_k/dx$. The force generated by each phase can be extracted through the phase current and translator position using the FEA resulted in curves shown in Fig. 1. Based on FEA, the inductances at various currents with respect to various translator positions are shown in Fig. 1(c).

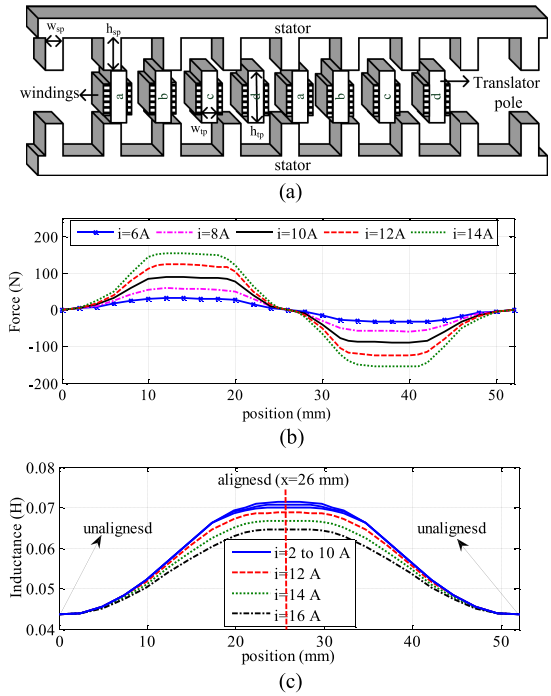

Fig. 1. (a) Proposed linear motor structure. (b) Phase force. (c) Inductance.

The inductances are about identical up to the rated current, but at higher currents due to saturation, its value decreases at the aligned position. The total propulsion force is the sum of forces of four phases

$$F_e = F_a\ + F_b + F_c + F_d. \tag{3}$$

While the force of phase *k* is expressed as

$$F\ (i_k, x) = \frac{\partial W_c\,(i_k, x)}{\partial x}\ = \frac{1}{2}\ \left(i_k^2\right) \frac{\partial L_k\,(x)}{\partial x} \tag{4}$$

where $W_c(i_k, x)$ indicates the electromagnetic energy. The total propulsion force $\mathrm{F_e}$ can be written as follows:

$$F_e = M\frac{d^2x}{dt^2} + C\frac{dx}{dt} + F_L \tag{5}$$

where M, C, and $\mathrm{F_L}$ represent the total mass of the moving part, friction coefficient, and external load force, respectively.

C. Control System

The block diagram of the proposed control system is shown in Fig. 2. The control system contains a speed controller with a current regulator, which could adjust the propulsion force directly. The reference force produced by the speed controller is divided between four phases using force distribution functions (FDFs). In this way, the reference forces of phases are obtained. According to the reference force and position of the translator, using FEA mentioned in Fig. 1, the reference currents are extracted.

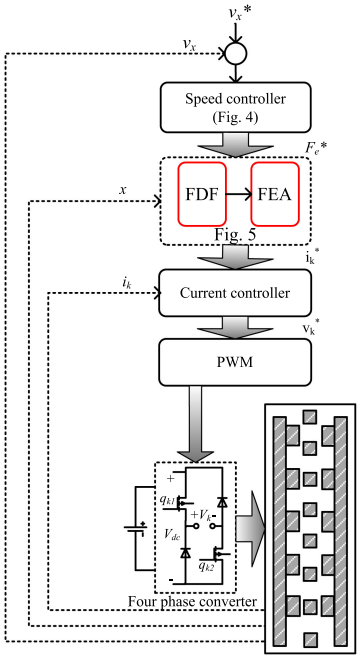

Fig. 2. LSRM and its control system.

III. Estimator

A. Kalman Filter (KF)

KF is an optimal method to predict the parameters of the system which could not be measured directly. It is used to obtain the best estimate of states based on previous knowledge of the system and measurement of states. Assume that the value of a parameter is written as

$$z_{j+1} = G_{j+1,\,j}\ .z_j + u_t \tag{6}$$

where z_j indicates the state vector at iteration j, G denotes the state transition matrix from iteration j to j+1, and u_t is a vector indicating the noise assumed to be zero-mean Gaussian with covariance matrix defined as

$$E\ \left\{u\left(n\right)u^T\left(j\right)\right\} = \begin{cases} Q\left(j\right) \text{ if } n = j \\ 0 \text{ if } n \neq j. \end{cases} \tag{7}$$

The measurements of the system can be written as

$$y_j = H_j\ .z_j + q_j \tag{8}$$

where y_j is a vector indicating the measurements of vector z at iteration j, matrix H maps the state vector into the measurement vector, and q_j indicates the associated measurement error that is assumed to be negligible. The state vector z_j is predicted and updated as follows:

$$\hat{z}_j^- = G_{j+1,j}\ .\hat{z}_{j-1}^- \tag{9}$$

$$P_j^- = G_{j+1,j}\ .P_{j-1}G_{j,\,j-1}^T + Q_{j-1}. \tag{10}$$

For accurate prediction, the state vector, the Kalman gain K, and the covariance matrix P_j should be updated as

$$K_j = P_j^-\ H_j^T\left[H_jP_j^-H_j^T + R_j\right]^{-1} \tag{11}$$

$$\hat{z}_j = \hat{z}_j^-\ + K_j\left(y_j - H_j\hat{z}_j^-\right) \tag{12}$$

$$P_j = \left(I - K_jH_j\ \right)\ P_j^-. \tag{13}$$

Optimal KF estimation for the state vector z_j can be reached if $z_{j\,=\,0}$, u_j, and q_j are normal random parameters. To update the Kalman parameter K in (11), it is necessary that $P(0) \neq 0$. The KF is appropriate for linear systems while most practical systems are nonlinear. For state estimation in a nonlinear system, a modified algorithm called extended Kalman filter (EKF) should be proposed.

B. Extended Kalman Filter

In this section, an EKF is presented, which is useful in the filtering problem in systems with nonlinear states and observations dynamics. Assuming that the system has no external inputs, and according to the nonlinear dynamics, we can write

$$z_{j+1} = g_j\ \left(z_j\right) + u_j \tag{14}$$

$$y_j = h_j\ \ \left(z_j\right) + q_j \tag{15}$$

where

$$z_j \in \mathcal{R}^n,\ g_j\left(z_j\right)\ :\ \mathcal{R}^n \to \mathcal{R}^n$$

$$y_j \in \mathcal{R}^r,\ h_j\left(z_j\right)\ :\ \mathcal{R}^n \to \mathcal{R}^r$$

$$q_j \in \mathcal{R}^r$$

$$u_j \in \mathcal{R}^n. \tag{16}$$

In the equations, $g_j(z_j)$ and $h_j(z_j)$ denote the time-dependent nonlinear transition function and nonlinear observation vector function, respectively. The system described by (14) and (15) should be linearized by

$$G_{j+1,\,j} = \frac{\partial g_j\left(z_j\right)}{\partial z}|_{z=\hat{z}_j} \tag{17}$$

$$H_{j+1,\,j} = \frac{\partial h_j\left(z_j\right)}{\partial z}|_{z=\hat{z}_j^-}. \tag{18}$$

After obtaining G and H, the nonlinear system is linearized around the current state estimate using the first term in the Taylor series

$$g_j\left(z_j\right) \approx G\left(z,\hat{z}_j\right) + G_{j+1,\,j}\left(z,\hat{z}_j\right) \tag{19}$$

$$h_j\left(z_j\right) \approx H\left(z,\hat{z}_j^-\right) + H_{j+1,\,j}\left(z,\hat{z}_j^-\right). \tag{20}$$

These equations are used to approximate the states (15) and (16). After the approximation, we can write

$$z_{j+1} \approx G_{j+1,\,j}.\ z_j + u_j + d_j \tag{21}$$

$$\bar{y}_j = H_j\ .z_j + q_j. \tag{22}$$

Parameters d_j and $\bar{y}_j$ are introduced as

$$d_j = \ G\left(z,\hat{z}_j\right) - G_{j+1,\,j}.\ \hat{z}_j \tag{23}$$

$$\bar{y}_j = y_j\ - \left\{h\left(z,\hat{z}_j^-\right) - H_j.\hat{z}_j^-\right\}. \tag{24}$$

Now, it is possible to predict the state vector of the system described in (14) and (15) as follows:

$$\hat{z}_j^- = g_j\ (\hat{z}_{j-1}) \tag{25}$$

$$\bar{P}_j = G_{j,j-1}\ P_{j-1} G_{j,j-1}^T - \left\{ h\left(z, \hat{z}_j^-\right) - H_j\ .\hat{z}_j^- \right\}. \tag{26}$$

The estimated parameters are updated by the following equations:

$$K_j = P_j^-\ H_j^T \left[H_j P_j^- H_j^T + R_j \right]^{-1} \tag{27}$$

$$\hat{z}_j = \hat{z}_j^-\ + K_j\ y_j - h_j\left(\hat{z}_j^-\right) \tag{28}$$

$$P_j = \ (I - K_j H_j\ )\ P_j^-. \tag{29}$$

C. Training Multilayer Perceptions (MLPs)

An MLP is a class of feedforward artificial neural networks, which uses a supervised learning technique for training. Its multiple layers and nonlinear activation distinguish MLP from a linear perception. It consists of some layers of nodes that represent artificial neural units. Each node calculates a weighted sum of inputs, with all nodes connected by links in the neighbor layer. If the EKF is applied, the states estimated by the filter are the network weights and the output of the MLP is the measurement utilized by the filter. In an estimation algorithm, optimization of the weights can be very effective in minimizing the prediction error. Assuming an MLP with *m* weights and *n* output nodes, the neural network can be written as follows:

$$z_{j+1} = z_j \tag{30}$$

$$\hat{y}_j = h\left(z_j,\ u_j\ \right) \tag{31}$$

where u_j and $\hat{y}_j$ denote the input vector and the output vector, respectively. In addition, z_j is the state vector and h indicates the nonlinear output function. According to (11)–(13) and (27)–(29), we can write

$$K_j = P_j\ H_j^T \left[H_j P_j H_j^T + R_j \right]^{-1} \tag{32}$$

$$z_{j+1} = z_j\ + \mu\ K_j\left[\ y_j - \hat{y}_j\right] \tag{33}$$

$$P_j = P_j\ - K_j H_j\ P_j + Q_j \tag{34}$$

where $P \in \mathcal{R}^{m\times m}$ and $K \in \mathcal{R}^{m\times n}$ are the matrices indicating the prediction error covariance and Kalman gain in the *j*th iteration, respectively. $Q \in \mathcal{R}^{m\times m}$, $R \in \mathcal{R}^{n\times n}$, and $H \in \mathcal{R}^{n\times m}$ are matrices that denote the noise covariance, error of measurement covariance, and partial derivative of each output of the neural network, respectively. Furthermore, μ is the learning rate, while *m* indicates the total number of weights. The derivative of the αth output of the neural network with respect to the βth weight is written as

$$H_{\alpha\beta} = \left[\frac{\partial \hat{y}_\alpha}{\partial z_\beta}\right]_{z_j = \hat{z}_{j+1}},\ \alpha\ =\ 1,\ \ldots,\ n,\ \beta\ =\ 1,\ \ldots,\ m. \tag{35}$$

Fig. 3 illustrates an MLP with $\mathrm{n_0}$ inputs, $\mathrm{n_h}$ nodes in the hidden layer, and one output node.

We can write the output of the system as

$$\sigma_\alpha = \frac{1}{1+e^{-\delta_\alpha}}\ \ \alpha\ =\ 1,\ \ldots,\ n_h \tag{36}$$

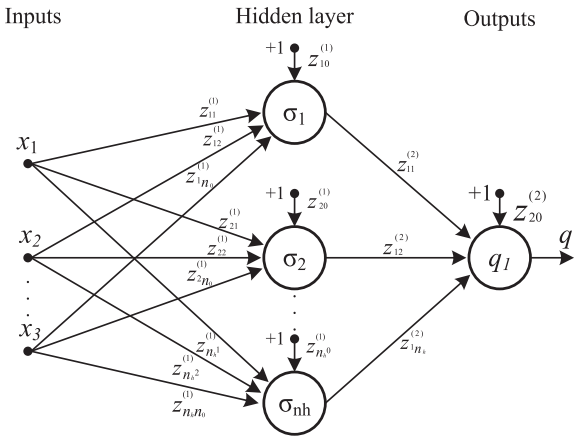

Fig. 3. Proposed MLP with layers.

$$\delta_\alpha = \sum_{\beta=0}^{n_0} z_{\alpha\beta}^{(1)}\ x_\beta\ \ x_0 = \ +1 \tag{37}$$

$$q_1 = \sum_{j=0}^{n_h} z_{1j}^{(2)}\ u_j\ \ u_0 = \ +1 \tag{38}$$

$$\hat{y} = q_1. \tag{39}$$

Then, matrix H can be written as

$$H\ = \frac{\partial \hat{y}}{\partial z}\ = \left[\frac{\partial \hat{y}}{\partial z_{10}^{(1)}}\ \frac{\partial \hat{y}}{\partial z_{11}^{(1)}}\ \cdots\ \frac{\partial \hat{y}}{\partial z_{1n_h}^{(2)}}\right]\ q_1 \tag{40}$$

where the components are as follows:

$$\frac{\partial \hat{\mathrm{y}}}{\partial \mathrm{z}_{10}^{(1)}} = \frac{\mathrm{z}_{11}^{(1)} \mathrm{e}^{-\delta_1}}{\left(1-\mathrm{e}^{-\delta_1}\right)^2}\ \mathrm{x}_0,$$

$$\frac{\partial \hat{\mathrm{y}}}{\partial \mathrm{z}_{11}^{(1)}} = \frac{\mathrm{z}_{11}^{(2)} \mathrm{e}^{-\delta_1}}{\left(1-\mathrm{e}^{-\delta_1}\right)^2}\ \mathrm{x}_1$$

$$\frac{\partial \hat{\mathrm{y}}}{\partial \mathrm{z}_{1\mathrm{n}_0}^{(1)}} = \frac{\mathrm{z}_{11}^{(2)} \mathrm{e}^{-\delta_1}}{\left(1-\mathrm{e}^{-\delta_1}\right)^2}\ \mathrm{x}_{\mathrm{n}_0}$$

$$\frac{\partial \hat{\mathrm{y}}}{\partial \mathrm{z}_{20}^{(1)}} = \frac{\mathrm{z}_{12}^{(2)} \mathrm{e}^{-\delta_2}}{\left(1-\mathrm{e}^{-\delta_2}\right)^2}\ \mathrm{x}_0$$

$$\frac{\partial \hat{\mathrm{y}}}{\partial \mathrm{z}_{21}^{(1)}} = \frac{\mathrm{z}_{12}^{(2)} \mathrm{e}^{-\delta_2}}{\left(1-\mathrm{e}^{-\delta_2}\right)^2}\ \mathrm{x}_1$$

$$\frac{\partial \hat{\mathrm{y}}}{\partial \mathrm{z}_{2\mathrm{n}_0}^{(1)}} = \frac{\mathrm{z}_{12}^{(2)} \mathrm{e}^{-\delta_2}}{\left(1-\mathrm{e}^{-\delta_2}\right)^2}\ \mathrm{x}_{\mathrm{n}_0}$$

$$\vdots$$

$$\vdots$$

$$\frac{\partial \hat{y}}{\partial z_{n_h 0}^{(1)}} = \frac{z_{1n_h}^{(2)} e^{-\delta_{n_h}}}{\left(1 - e^{-\delta_{n_h}}\right)^2} x_0$$

$$\frac{\partial \hat{y}}{\partial z_{21}^{(1)}} = \frac{z_{1n_h}^{(2)} e^{-\delta_{n_h}}}{\left(1 - e^{-\delta_{n_h}}\right)^2} x_1$$

$$\frac{\partial \hat{y}}{\partial z_{2n_0}^{(1)}} = \frac{z_{1n_h}^{(2)} e^{-\delta_{n_h}}}{\left(1 - e^{-\delta_{n_h}}\right)^2} x_{n_0}$$

$$\frac{\partial \hat{y}}{\partial z_{10}^{(2)}} = 1, \quad \frac{\partial \hat{y}}{\partial z_{11}^{(2)}} = \frac{1}{1 + e^{-\delta_1}}$$

$$\frac{\partial \hat{y}}{\partial z_{1n_h}^{(2)}} = \frac{1}{1 - e^{-\delta_{n_h}}}.$$

Finally, we can express H for the proposed MLP as follows:

$$H = [\gamma(\delta_1) x_0 \ldots \gamma(\delta_1) x_{n_0} \gamma(\delta_2) x_0 \ldots \gamma(\delta_{n_h}) \; x_{n_0} u_0 u_1 \ldots u_{n_h}] \tag{42}$$

where

$$\gamma(\delta_\alpha) = \frac{z_{1\alpha}^{(2)} e^{-\delta_\alpha}}{(1 + e^{-\delta_\alpha})^2} \quad \alpha = 1, \ldots, n_h. \tag{43}$$

IV. Proposed Control Strategy for the LSRM

The proposed strategy shown in Fig. 2 controls the speed, force, and phase current of the LSRM simultaneously. The output of the speed control unit inters to the force control unit which creates phase forces by FDFs and position data. The article shows that a high-speed controller without time delay has a favorable effect on the overall output of the system. Therefore, the use of the proposed method to control the motor speed makes it possible to suddenly change and rapidly increase the phase current ad phase force. In this way, the force drop during the commutation of the phases is partially compensated and the ripple is reduced.

A. Speed Controller

To achieve a smooth and efficient motion, the command linear speed v_x^* is created by a jerk minimization profile discussed in [7]. Dynamic equations of the LSRM can be written as follows:

$$\dot{x} = v. \tag{44}$$

It indicates the speed as the time derivative of position. Another equation is obtained using (3) as

$$\dot{v} = -\frac{C + k_p}{M} v + \frac{1}{M} F_e \tag{45}$$

where k_p is a constant factor and $F_L = k_p \frac{dx}{dt} = k_p v$. We can write the dynamic equations in matrix form as follows:

$$\begin{bmatrix} \dot{x}_1 \\ \dot{x}_2 \end{bmatrix} = \begin{bmatrix} \dot{x} \\ \dot{v} \end{bmatrix} = \begin{bmatrix} 0 & 1 \\ 0 & -\frac{C+k_p}{M} \end{bmatrix} \begin{bmatrix} x_1 \\ x_2 \end{bmatrix} + \begin{bmatrix} 0 \\ \frac{1}{M} \end{bmatrix} [F_e]. \tag{46}$$

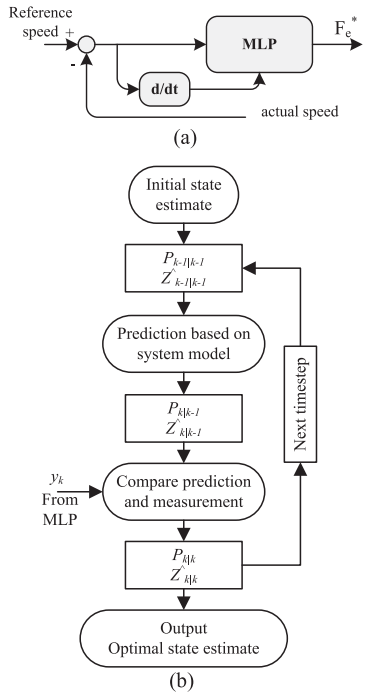

Fig. 4. (a) MLP used for speed control. (b) EKF and MLP combination.

The MLP illustrated in Fig. 3 is used to implement the proposed control method as displayed in Fig. 4. The MLP algorithm has two inputs including position error and speed error of the LSRM. The errors are obtained by comparing the actual values with the corresponding command values. Furthermore, the network contains a hidden layer with ten nodes and one neuron at the output layer. The process in the proposed MLP is estimated by EKF as shown in Fig. 4. The MLP shown in Fig. 3 is formed with the translator position and speed errors as inputs. Hidden layer calculations are done based on the equations mentioned in Section III. The output of the MLP is obtained by (45), which is the input of the force control unit.

B. Force Controller

The LSRM phases must be turned ON and OFF accurately so that the command propulsion force is provided. Using the proposed control strategy, two phases can be turned ON simultaneously. This enhances the propulsion force density [25]. The command force obtained from the speed controller enters the force control block. Multiplying the input by the FDFs presented in [7], the command phase forces are determined where the command currents can be obtained once the position is known.

C. Current Controller

Due to the effect of the current on the propulsion force generation, it is very important to minimize the current errors. This can be done using an appropriate current controller. The output of the force control block includes reference currents of four phases which must be provided to eventually produce the desired force. Comparing the reference and actual current values, the error is given to a conventional PI controller. In this article,

TABLE I
PARAMETERS OF THE PROPOSED LSRM

variable	Symbol	Value
Air gap length (mm)	g	2
Stator pole width (mm)	w_{sp}	21
Stator slot width (mm)	w_{ss}	31
Stator pole height (mm)	h_{sp}	30
Translator pole width (mm)	w_{tp}	13
Translator pole height (mm)	h_{tp}	26
Winding turns		200
Rated current (A)	i_{rated}	10
Rated voltage V)	v_{rated}	150
Coefficient of friction	C	20 N/m/s
Weight of translator (M)	M	7 kg
Phase resistance	R	2.5 Ω

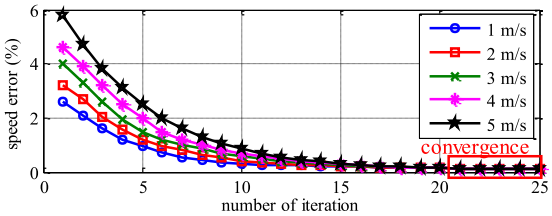

Fig. 5. Change in speed error in the training iteration.

2.2 kHz and 1.5 were selected for the bandwidth and damping ratio of the controller based on the trial and error method.

V. SIMULATION EVALUATIONS

In this section, the performance of the LSRM using the proposed control strategy is presented. For a more complete study, the results obtained by the controller are compared by the findings obtained by two other controllers: a conventional PI controller and an adaptive fuzzy (AF) control system presented in [11]. Modeling of the LSRM has been done in MATLAB/Simulink software based on data extracted from FEA. Parameters of the motor are shown in Table I.

In the proposed control strategy, where an EKF was used for training, the iteration is finished when the error between the predicted and measured speed values fall below less than 0.1%. Fig. 5 indicates the speed error in percentage in the training iteration. The convergence of the speed error occurs at training 21–25.

Initially, the performance of the system has been studied at different speeds with its results illustrated in Fig. 6. In all studies, the acceleration is set to 1 m/s^2. Speed profiles are shown in Fig. 6(a), whereas the corresponding force profiles are indicated in Fig. 6(b). The total propulsion force and four phases force at speed 3 m/s are shown in Fig. 6(c). The current in the output of the source along with two phase currents is illustrated in Fig. 6(d).

To explore the performance of the controller under load conditions, a nominal load is applied to the motor at $t = 3$ s. The obtained results are shown in Fig. 7. As the load is applied,

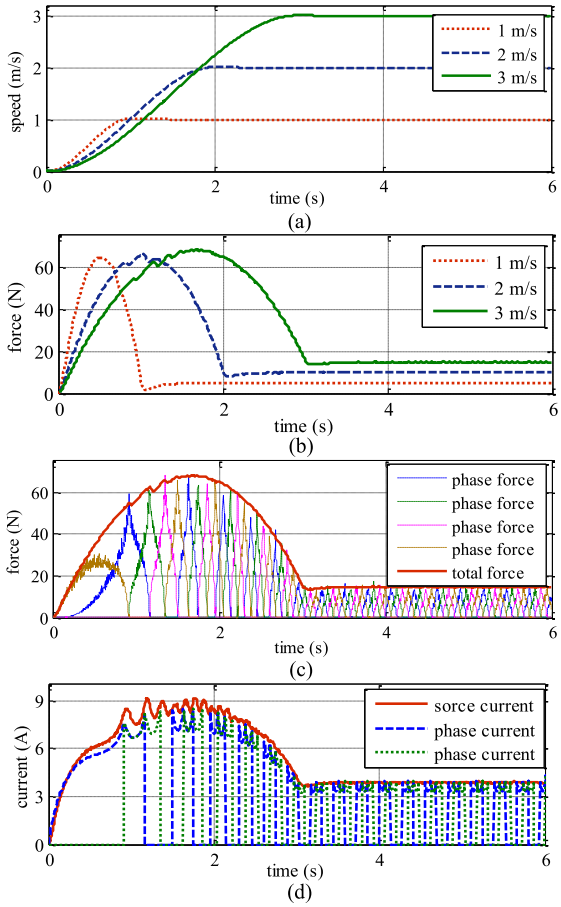

Fig. 6. Proposed control strategy—no load condition. (a) Various speeds. (b) Propulsion force at different speeds. (c) Phase forces and total force at 3 m/s. (d) Source current and phase current at 3 m/s.

the speed drops slightly while the propulsion force increases to maintain the previous speed. The speed error between the reference and actual values is shown in Fig. 7(b). In the illustrations, the ripple of speed at steady state (*rs*), overshoot of speed at load application (*os*), settling time of the speed (*ts*), and ripple of force (*rf*) are specified in Fig. 7.

A comparison of speed ripple and speed overshoot for three control strategies has been demonstrated in Fig. 8. These results have been extracted at speed of 1 m/s with the nominal load. The simulation results for other speeds can be seen in Fig. 9. The results confirm that the proposed controller outperformed the other strategies.

The MLP weights are the states that the EKF estimates, whereas the output of the MLP is the measurement command force utilized by the EKF. This is shown in Fig. 4 as y_k. With the optimal weights, the error between the measurement and prediction values would be minimized. The error at speed 1 m/s for three iterations is shown in Fig. 10. It can be seen that after 25 iterations, the error is acceptable. These results confirm the ability of the EKF in the estimation of the MLP weights.

Due to the parameter uncertainty in an SRM, the conventional PI controller leads to less accurate results. This can be seen both in the average value and in the ripple. The adaptive fuzzy

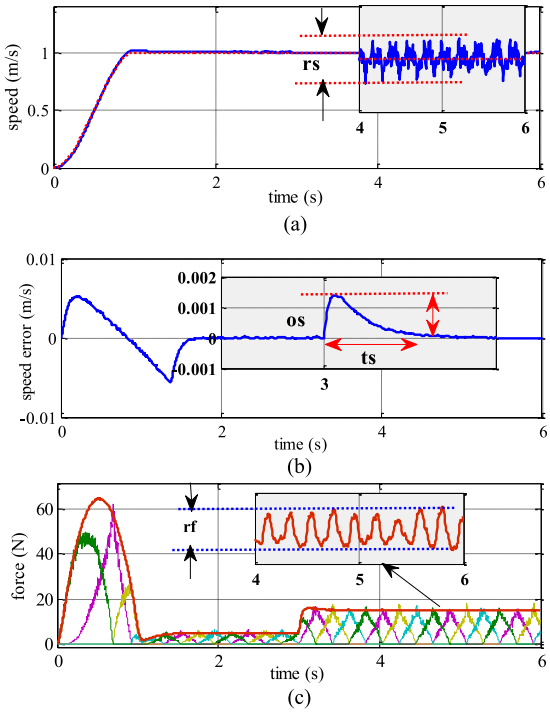

Fig. 7. Proposed control strategy—load condition. (a) Speed and ripple. (b) Speed error. (c) Force at 1 m/s.

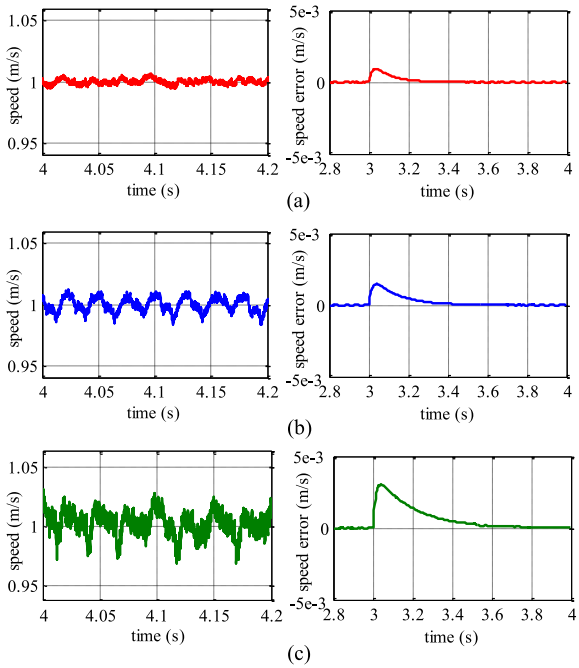

Fig. 8. Methods comparison under load condition. (a) Proposed method. (b) AF method. (c) PI method.

control method presented in [11] shows better results than the PI method. The accuracy of this method can be increased by adding more membership functions. However, this makes the system more complex and slow, which leads to some errors. The proposed method can adapt to unmodeled dynamics and parameter uncertainties without the need of having a complete

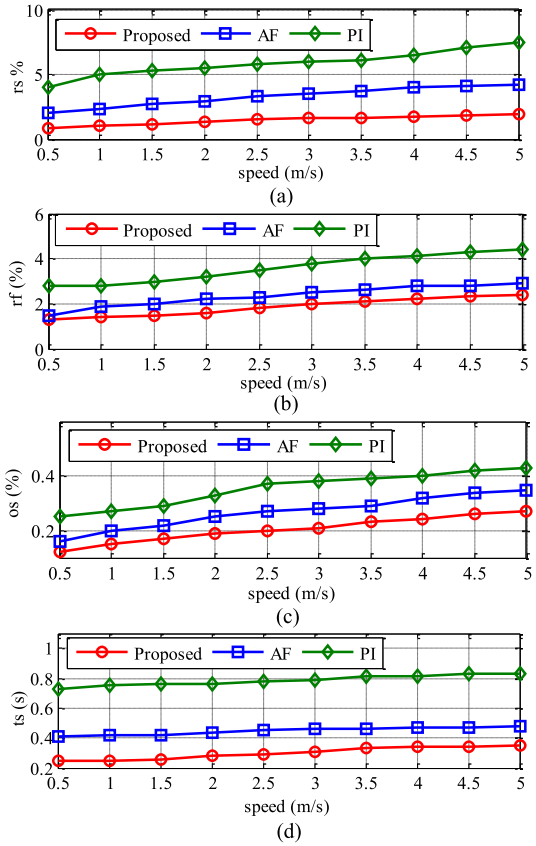

Fig. 9. Proposed control strategy. (a) Ripple of speed. (b) Ripple of force. (c) Overshoot of speed at loading. (d) Settling time.

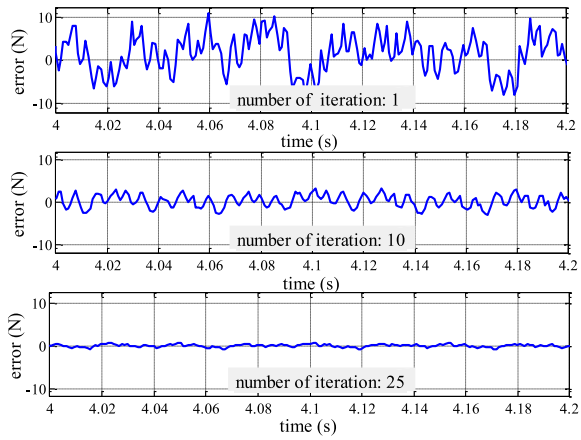

Fig. 10. Error between the measured and predicted values.

dataset. These lead to better results compared to the other two methods.

The proposed LSRM has a large air gap of 2 mm and does not have any saturation problem. Therefore, according to Fig. 1, the inductances are identical in all different currents up to the rated current 10 A. However, to reveal the level of saturation, the motor performance has been investigated when the current is above the rated value. The motor is started to reach the desired speed of 5 m/s. At $t = 5$ s, the nominal load is applied to the motor, whereas, at t = 7.5 s, the load is doubled. Fig. 11 shows the

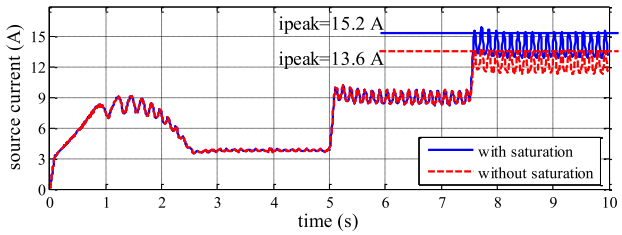

Fig. 11. Proposed control strategy with and without saturation.

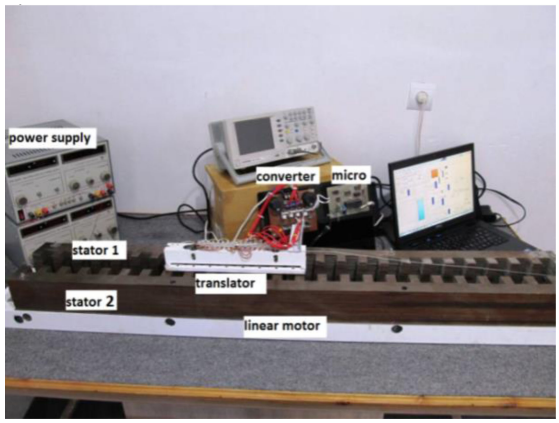

Fig. 12. Schematic diagram of the prototype system.

input current of the power converter with and without saturation consideration.

VI. Experimental Evaluations

The prototype is manufactured and an experimental setup shown in Fig. 12 is built to test the proposed system. The output of the converter is controlled by an ARM Cortex-M4 microcontroller STM32f407 with 72 MHz processing frequency. Phase currents are measured by Hall sensors. Also, displacement and speed signals are obtained by a magnetic sensor strip with 10 μm resolution runs alongside the stator and a capture channel of the timer inside the microcontroller, respectively. All signals were stored in the external memory of the microcontroller every 10 ms and are called from it. Thus, instantaneous parameters sampling data synchronized with each control loop time (1 ms) cannot be shown in experimental results. Therefore, the experimental data stored in memory are transferred to the software to draw curves.

The control method was implemented in the software and applied to the LSRM. In addition, two other strategies, an adaptive fuzzy control method described in our previous work [11] and a conventional PI method, were applied and the obtained results were compared. The measured speeds of the motor along with the corresponding propulsion forces are depicted in Fig. 13. These curves are related to the proposed strategy while its comparison with the other methods is given in Table II. Currents obtained in the three mentioned speeds are also shown in Fig. 13. Zoomed in speed and force curves at speed 1 m/s for the proposed method are shown in Fig. 14.

Figs. 13 and 14 prove that the proposed control method has an acceptable ability in the LSRM control. Moreover, a comparison

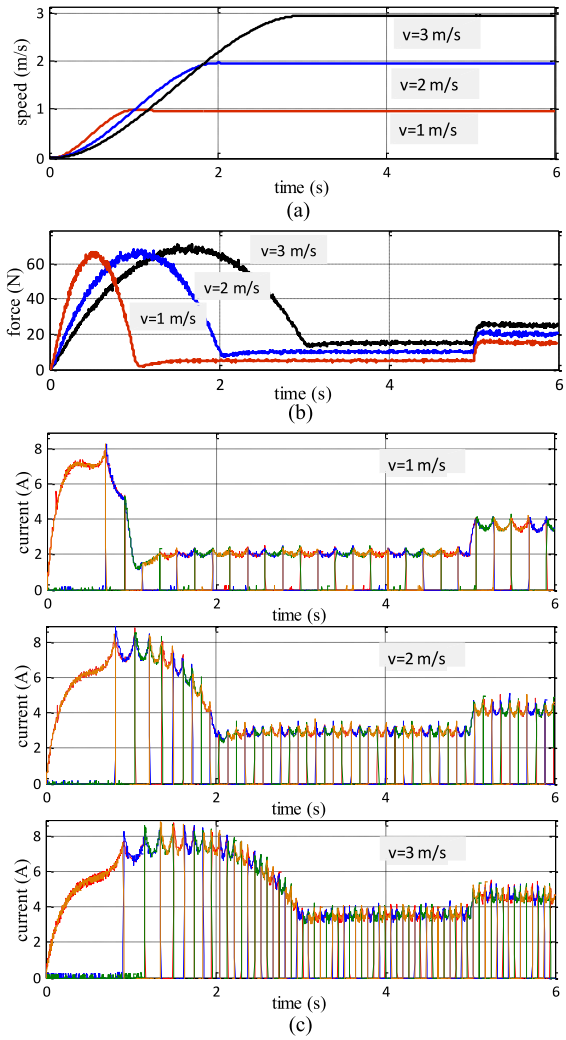

Fig. 13. Experimental results. (a) Speed. (b) Forces. (c) Currents.

TABLE II
Experimental Results Comparison

Controller		parameters			
Speed (m/s)		rs (%)	rf (%)	os (%)	ts (s)
Proposed controller	1	1.4	1.5	0.12	0.23
	2	1.6	1.6	0.20	0.27
	3	1.9	2.0	0.22	0.31
Adaptive fuzzy	1	2.2	2.0	0.20	0.41
	2	2.7	2.2	0.26	0.43
	3	3.1	2.4	0.28	0.44
PI	1	5	2.9	0.28	0.68
	2	5.8	3.2	0.32	0.68
	3	6.2	3.9	0.38	0.70

of the results obtained by two other control strategies in Table II confirms that the proposed method is superior to the other methods.

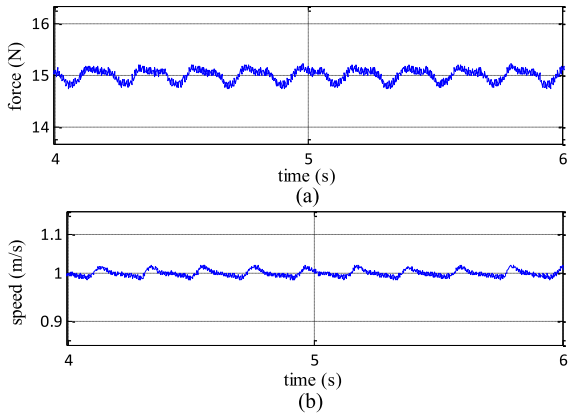

Fig. 14. Experimental results at 1 m/s. (a) Force ripple. (b) Speed ripple.

VII. Conclusion

SRMs are inherently nonlinear systems and their control is more difficult than the other electrical machines. The conventional control methods often have problems in these cases. In this article, an adaptive PID controller is used to regulate the speed of a linear SRM. To simplify the analytical calculations of partial derivatives, an MLP is added to the conventional controller, which requires a complete dataset of the system output. To overcome the problem, an EKF is used to estimate uncertain parameters. Eventually, the proposed control strategy can process data and predict the next values in a limited time without the complete observations. The proposed method and two other strategies have been applied to a linear motor and their performance has been compared by the simulation and experimental tests.

Acknowledgment

This publication was made possible by Qatar University NPRP11s1125-170027 from the Qatar University. The statements made herein are solely the responsibility of the authors.

References

[1] H. S. Lim, R. Krishnan, and N. S. Lobo, "Design and control of a linear propulsion system for an elevator using linear switched reluctance motor drives," *IEEE Trans. Ind. Electron.*, vol. 55, no. 2, pp. 534–542, Feb. 2008.

[2] X. Sun, K. Diao, G. Lei, Y. Guo, and J. Zhu, "Real-time HIL emulation for a segmented-rotor switched reluctance motor using a new magnetic equivalent circuit," *IEEE Trans. Power Electron.*, vol. 35, no. 4, pp. 3841–3849, Apr. 2020.

[3] S. J. Evangeline, K. Venmathi, and S. Ajayan, "Speed control of switched reluctance motor using fractional order control," in *Proc. Int. Conf. Innov. Elect., Electron., Instrum. Media Technol.,* 2017, pp. 367–372.

[4] W. Lei, C. Li, and M. Z. Q. Chen, "Robust adaptive tracking control for quadrotors by combining PI and self-tuning regulator," *IEEE Trans. Control Syst.*, vol. 27, no. 6, pp. 2663–2671, Nov. 2019.

[5] R. Errouissi, A. Al-Durra, and S. M. Muyeen, "Experimental validation of a novel PI speed controller for AC motor drives with improved transient performances," *IEEE Trans. Control Syst.*, vol. 26, no. 4, pp. 1414–1421, Jul. 2018.

[6] Y. I. Son, I. H. Kim, D. S. Choi, and H. Shim, "Robust cascade control of electric motor drives using dual reduced-order PI observer," *IEEE Trans. Ind. Electron.*, vol. 62, no. 6, pp. 3672–3682, Jun. 2015.

[7] S. Masoudi, M. R. Feyzi, and M. B. B. Sharifian, "Force ripple and jerk minimization in double sided linear switched reluctance motor used in elevator application," *IET Electr. Power. Appl.*, vol. 10, no. 6, pp. 508–516, Jul. 2016.

[8] Z. Yu, C. Gan, Y. Chen, and R. Qu, "DC-biased sinusoidal current excited switched reluctance motor drives based on flux modulation principle," *IEEE Trans. Power Electron..*, vol. 35, no. 10, pp. 10614–10628, Oct. 2020.

[9] C. Gan, F. Meng, Z. Yu, R. Qu, Z. Liu, and J. Si, "Online calibration of sensorless position estimation for switched reluctance motors with parametric uncertainties," *IEEE Trans. Power Electron.*, vol. 35, no. 11, pp. 12307–12320, Nov. 2020.

[10] D. Xiao, J. Ye, G. Fang, Z. Xia, X. Wang, and A. Emadi, "Improved feature-position-based sensorless control scheme for SRM drives based on nonlinear state observer at medium and high speeds," *IEEE Trans. Power Electron.*, vol. 36, no. 5, pp. 5711–5723, May 2020.

[11] S. Masoudi, M. R. Soltanpour, and H. Abdollahi, "Adaptive fuzzy control method for a linear switched reluctance motor," *IET Electr. Power. Appl.*, vol. 12, no. 9, pp. 1328–1336, Aug. 2018.

[12] A. Azadrou, S. Masoudi, R. Ghanizadeh, and P. Alemi, "New adaptive fuzzy sliding mode scheme for speed control of linear switched reluctance motor," *IET Electron. Power Appl.*, vol. 13, no. 8, pp. 1141–1149, Aug. 2019.

[13] W. Lei, C. Li, and M. Z. Q. Chen, "Robust adaptive tracking control for quadrotors by combining PI and self-tuning regulator," *IEEE Trans. Control Syst. Technol.*, vol. 27, no. 6, pp. 2663–2671, Nov. 2019.

[14] M. H. Khooban, O. Naghash-Almasi, T. Niknam, and M. Sha-Sadeghi, "Intelligent robust PI adaptive control strategy for speed control of EV(s)," *IET Sci. Meas. Technol.*, vol. 10, no. 5, pp. 433–441, Jul. 2016.

[15] J. Wang, "Speed-assigned position tracking control of SRM with adaptive backstepping control," *IEEE/CAA J. Autom. Sin.,* vol. 5, no. 6, pp. 1128–1135, Nov. 2018.

[16] M. Dursun and S. Ozden, "GA based adaptive velocity control of linear switched reluctance motor under different load and velocity profiles for industrial application," in *Proc. 2nd Int. Conf. Control, Autom. Robot.,* Apr. 2016, pp. 124–127.

[17] P. Azer, B. Bilgin, and A. Emadi, "Comprehensive analysis and optimized control of torque ripple and power factor in a three-phase mutually coupled switched reluctance motor with sinusoidal current excitation," *IEEE Trans. Power Electron.*, vol. 36, no. 6, pp. 7150–7164, Jun. 2021.

[18] P. Azer, S. Nalakath, and A. Emadi, "Model-based spatial harmonics vector compensation method for three-phase mutually coupled switched reluctance machine with sinusoidal current excitation," *IEEE Open J. Power Electron.*, vol. 1, pp. 216–226, 2020.

[19] Z. Yin, F. Gao, Y. Zhang, C. Du, G. Li, and X. Sun, "A review of nonlinear Kalman filter applying to sensorless control for AC motor," *CES Trans. Elect . Mach. Syst.*, vol. 3, no. 4, pp. 351–362, Dec. 2019.

[20] E. Quintero-Manriquez, E. N. Sanchez, R. G. Harley, S. Li, and R. A. Felix, "Neural inverse optimal control implementation for induction motors via rapid control prototyping," *IEEE Trans. Power Electron.*, vol. 34, no. 6, pp. 5981–5992, Jun. 2019.

[21] M. Stender, O. Wallscheid, and J. Bocker, "Accurate torque control for induction motors by utilizing a globally optimized flux observer," *IEEE Trans. Power Electron.*, vol. 36, no. 11, pp. 13261–13274, Nov. 2021.

[22] L. Yu-Zhou and Z. Ke-Gang, "Sensorless speed control of the switched reluctance motor using extended Kalman filter," in *Proc. 2nd Int. Conf. Inf. Sci. Eng.*, Dec. 2010, pp. 2375–2378.

[23] Y. Saadi, R. Sehab, A. Chaibet, M. Boukhnifer, and D. Diallo, "Sensorless control of switched reluctance motor with unknown load torque for EV application using extended Kalman filter and second order sliding mode observer," in *Proc. IEEE Int. Conf. Ind. Technol.*, Feb. 2018, pp. 522–528.

[24] D. M. Araujo, F. T. Simo, and Y. Perriard, "General sensorless method with parameter identification and double Kalman filter applied to a bistable fast linear switched reluctance actuator for textile machine," *IEEJ J. Ind. Appl.*, vol. 8, no. 1, pp. 33–40, 2019.